IEEE Access
Multidisciplinary | Rapid Review | Open Access Journal

Received 16 July 2024, accepted 6 August 2024, date of publication 13 August 2024, date of current version 26 August 2024.

Digital Object Identifier 10.1109/ACCESS.2024.3443152

RESEARCH ARTICLE

Optimizing Multi-Timescale Scheduling of Combined Cooling, Heating, and Power Systems Under Penalty-Reward Tiered Carbon Trading

TIANYI MA, YILIN WANG, TING LI, (Member, IEEE), YUHAO ZHANG, AND ZHIYUAN WANG

School of Mechanical and Electrical Engineering, Beijing Institute of Graphic Communication, Beijing 102600, China

Corresponding author: Tianyi Ma (matianyi@bigc.edu.cn)

This work was supported in part by the Research and Development Program of Beijing Municipal Education Commission under Grant KM202310015003.

ABSTRACT As the penetration of global new energy into power systems increases, the impact of carbon trading on energy systems continues to grow. Therefore, it is crucial to study the effects of carbon trading mechanisms on the operational characteristics of power systems that include new energy sources. This paper focuses on China, the world's largest energy-consuming economy, and proposes a multi-time-scale optimization scheduling method for a Combined Cooling, Heating, and Power (CCHP) system that considers a reward-penalty tiered carbon trading mechanism. This method effectively enhances the economic, environmental, and stability performance of the CCHP system. Firstly, the relationship between different carbon trading mechanisms and carbon trading volumes is analyzed to identify the carbon trading mechanism with the highest correlation to economic efficiency. Based on this analysis, a carbon trading model is introduced into the system's economic dispatch strategy, constructing an economic model for the CCHP system under the influence of the carbon trading mechanism. While considering economic efficiency, this study also aims to improve system stability by proposing a multi-time multi-layer rolling optimization scheduling method. This method adjusts equipment output to respond to random fluctuations caused by uncertainties in energy sources and loads. The optimization results of the case study show that the introduction of the reward-penalty tiered carbon trading mechanism can reduce the carbon emissions of the park and improve economic performance. Additionally, the multi-time multi-layer rolling optimization scheduling effectively mitigates random fluctuations in supply and demand, ensuring stable system operation.

INDEX TERMS Combined cooling, heating, and power (CCHP) system, carbon trading mechanism, carbon emissions, reward-penalty tiered carbon trading, multi-timescale optimization scheduling.

I. INTRODUCTION

The increasing global carbon emissions and resulting climate change pose significant threats to economic and social development, human health, and even survival. According to data analysis from the National Aeronautics and Space Administration (NASA), global temperatures and Arctic sea ice extent broke multiple records in the first half of 2016. Global climate change is projected to cause incalculable losses and impose substantial costs on humanity. The urgent need to control carbon emissions has been widely accepted worldwide.

Carbon trading is a crucial climate policy adopted by many countries and regions to regulate carbon emissions. The European Union Emissions Trading System (EU ETS), established on January 1, 2005, aims to achieve CO2 emission reduction targets set by the Kyoto Protocol. Its purpose is to internalize environmental costs by transforming the environment into a compensated production factor through market mechanisms. By establishing the European Union Allowance (EUA) trading market, it effectively allocates environmental

The associate editor coordinating the review of this manuscript and approving it for publication was Gaetano Zizzo.

resources, promotes the development of energy-saving and emission-reducing technologies, and minimizes operational costs for enterprises under climate protection efforts. Additionally, carbon trading markets in countries such as Australia, South Korea, and Japan are steadily developing. It is evident that carbon trading, as a significant climate policy for greenhouse gas emission control, has gained widespread recognition among major countries worldwide.

In 2020, the Chinese government presented the 'Dual Carbon' policy at the 75th United Nations General Assembly, with the objective of reaching the peak of carbon dioxide emissions by 2030 and attaining carbon neutrality by 2060 [1]. The power industry, which is a major source of carbon emissions [2], has a crucial influence on the development of China's future strategies for reducing carbon emissions through its energy utilization and adjustments.

The endeavor to improve the energy efficiency and reduce carbon emissions in power systems has motivated many researchers to investigate various methods and mechanisms for carbon reduction. Carbon dioxide (CO2) emissions are considered as a dispatchable resource [3]. A preliminary model for low-carbon power dispatch deci-sion-making has been developed to integrate 'electric balance' and 'carbon balance' in power dispatch, taking into account various factors such as low-carbon power technologies, carbon costs, and constraints. Additionally, many studies discuss methodologies related to policy mechanisms like carbon taxes and carbon trading [4], [5]. Xuan et al. [4] demonstrates that the incorporation of carbon taxes in economic dispatch models affects the generation output of all units, leading to a reduction in carbon emissions. This is evident through a comparison of economic dispatch scenarios with and without carbon taxes. Yao et al. [5] presents a commercial model for carbon capture, utilization, and storage within the context of carbon markets and policies. The model integrates carbon penalties and revenues into the objective function to represent the uncertainty associated with carbon taxes and prices. Wu et al. [6] undertakes an analysis and comparison of benchmark carbon pricing models and tiered carbon pricing models, aiming to establish the relationship between carbon trading costs and carbon trading volumes. Yang et al. [7] delineates the framework of carbon trading markets and formulates a model for estimating carbon trading expenses through an examination of carbon emissions and emission quotas.

The carbon trading mechanism is effective in reducing carbon emissions within systems. As research advances, the conventional single carbon pricing mechanism has transformed into a tiered carbon trading system. It has been widely applied in the scheduling of low-carbon economies within energy systems [8], [9], [10], [11], [12], [13], [14], [15], [16], [17], [18], [19]. Zhu et al. [8] presents an optimization scheduling model that takes into account demand response and participation in power-to-gas (P2G) within the carbon trading market. The traditional carbon trading mechanism demonstrates that a rational carbon pricing strategy can effectively promote low-carbon economic activities within systems. Wang et al. [9] presents a tiered carbon trading mechanism and develops a low-carbon economic scheduling model for a microgrid, with the goal of minimizing both operational expenses and carbon trading costs. This accomplishes the twin goals of decreasing operational expenses and carbon emissions. Zhou et al. [10] introduces a low-carbon economic operational strategy for a multi-agent integrated energy system. The strategy is based on a two-stage tiered carbon trading model with quota sharing mechanisms, aimed at ensuring the system's low carbon footprint, economic efficiency, and effectiveness. Furthermore, the carbon trading mechanism introduced in Wang et al. [11] is tiered. A low-carbon optimization scheduling model is developed with the objective of minimizing the total costs associated with energy purchases, carbon emission trading, equipment maintenance, and demand response. This model improves the dependability, cost-effectiveness, and environmentally friendly characteristics of integrated energy systems. However, although these studies present carbon trading models, they offer limited analysis of the correlation mechanisms between emissions and carbon trading market prices. They also fail to consider the influence of carbon trading mechanisms on the impact of renewable energy usage in energy systems. These systems may encounter diminished stability as a result of the extensive incorporation of renewable energy, leading to heightened volatility within the system under the impact of carbon trading mechanisms.

Numerous studies focused on examining the uncertainty in source-load dynamics within energy systems that incorporate renewable energy sources, in order to effec-tively improve the stability of energy systems in the context of carbon trading mechanisms [20], [21], [22], [23]. Wang et al. [20] presents a three-stage mixed time-scale rolling optimization approach that effectively addresses variations in both loads and renewable energy output. Additionally, a multi-timescale optimization operational method is pro-posed [21], which involves 'day-ahead - intra-day-real-time adjustment'. This approach not only improves the operational efficiency of combined cooling, heating, and power (CCHP) systems but also mitigates equipment power fluctuations and operational losses. In a similar manner, Zhou et al. [22] seeks to minimize overall operational costs and introduces a multi-timescale regional comprehensive energy system scheduling model. This model accomplishes both the economic and stable operation of regional comprehensive energy systems. The multi-time scale optimization method has been shown to effectively enhance system stability. Some studies have integrated this approach with carbon trading mechanisms, achieving low-carbon economic efficiency in energy systems while also ensuring system reliability [24], [25], [26], [27].

The existing body of research predominantly concentrates on the integration of carbon trading mechanisms into diverse

energy systems with the aim of mitigating carbon emissions. However, there is a deficiency in comprehensive analysis of the operational interplay between carbon trading mechanisms and energy systems. Furthermore, there is a limited number of studies that have integrated carbon trading mechanisms into multi-timescale optimization scheduling models aimed at achieving a balance between decreased carbon emissions and operational costs, while also ensuring system stability.

While carbon trading policies vary among countries, their essence lies in buying or selling carbon allowances to incentive reductions in carbon emissions. China, as a major consumer of energy with a prominent position in non-renewable energy consumption globally and the largest installed capacity of renewable energy, plays a crucial role in global energy systems. Therefore, studying the impact of China's carbon trading mechanisms on energy systems is highly relevant for global energy transitions. Consequently, this paper focuses on studying the energy system of a specific industrial park in China, systematically analyzing the correlation mechanisms between park emissions and transaction prices in the carbon trading market. The text presents a mathematical model for energy systems in industrial parks, taking into account the impact of a reward-penalty tiered carbon trading mechanism. Based on the analysis conducted, a scheduling algorithm for multi-layer, multi-timescale optimization is proposed. This algorithm not only aims to maximize the utilization of renewable energy sources, but also takes into account the uncertainty associated with both renewable energy and load demand. By maintaining a balance between supply and demand and reducing the unpredictable fluctuations in supply and demand, this approach effectively improves the stability of the energy system in the industrial park, while also preserving economic efficiency and minimizing carbon emissions.

II. CORRELATION BETWEEN INDUSTRIAL PARK EMISSIONS AND CARBON TRADING MARKET TRANSACTION PRICES

The fundamental purpose of the carbon trading mechanism within the industrial park is to create a market for carbon trading, enabling participation from carbon-emitting enterprises and users. The park's carbon emissions are controlled through the trading of carbon emission rights in the market, employing economic mechanisms. The operational process of the carbon trading mechanism specifically entails the establishment of legitimate carbon emission rights. It allows producers to participate in the trading of carbon emission rights in the market in order to accomplish emission control goals. At the outset, government authorities assign carbon emission quotas to each source of emissions. Producers subsequently adjust their production and emissions to conform to their assigned quotas. If the actual carbon emissions are lower than the allocated quotas, excess quotas can be exchanged in the carbon trading market. Conversely, in the event that emissions surpass the allocated quotas, it becomes necessary to procure extra carbon emission allowances Fig. 1 illustrates the model of the carbon trading system.

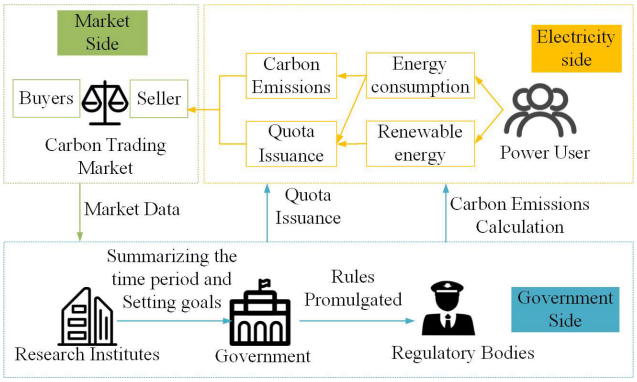

FIGURE 1. Carbon trading system model.

A. CARBON EMISSIONS

The carbon emissions of CCHP system in the park primarily stem from three sources: electricity, gas, and heat. The thermal load in the system is supplied by electricity and natural gas, and the actual carbon emissions Q_C^t at time t can be calculated using the following equation:

$$Q_C^t = Q_E^t + Q_G^t \tag{1}$$

where Q_E^t denotes the carbon emissions generated from purchasing electricity from the grid; and Q_G^t denotes the carbon emissions of equipment using natural gas as the primary energy source.

$$Q_E^t = \delta_E \cdot \sum_{t=1}^{k} P_E^t \tag{2}$$

$$Q_G^t = \delta_G \cdot \sum_{t=1}^{k} M_G^t \tag{3}$$

where δ_E denotes the carbon emission factor per unit of electricity from the regional grid in which the system is located; δ_G denotes the carbon emission factor for natural gas; P_E^t denotes the power exchange between the system and the grid at time t; and M_G^t denotes the amount of natural gas input into the system at time t.

B. CARBON TRADING QUOTA

Two prevalent methods of carbon quota allocation in the current market are free allocation and paid allocation. The process of paid allocation primarily involves an objective reality through auctioning, which requires systems to pay corresponding fees for their carbon emissions. "Free allocation" pertains to the advance allocation of com-plimentary carbon emission quotas to entities, with the objective of bolstering their incentive to participate.

When determining carbon emission quotas, two predominant approaches are commonly used: one based on historical emissions and the other on bench-marking. Obtaining historical emission data from companies can be challenging. This paper adopts the bench-marking method as the primary approach for determining quotas in the power industry, specifically focusing on establishing carbon emission quotas.

In China, the carbon trading mechanism is presently in an exploratory phase, and the allocation of complimentary quotas varies among different power plants. The carbon emission allowances for the electricity generation of gas turbines can be transformed by considering the quantity of heat provided. This process entails the conversion of electricity generation into heat units, which are then combined with the original heat supply to calculate the total heat. Subsequently, this total heat is utilized for quota allocation. With regard to GB, their allocation of quotas is determined exclusively by their heat output, as demonstrated in Equation (4).

$$Di = \begin{cases} \lambda_r \cdot (P_{Ri} + \beta P_{Ei}) & \textit{the gas unit } i \textit{ is a gas turbine} \\ \lambda_r \cdot P_{Ri} & \textit{the gas unit } i \textit{ is a gas boiler} \end{cases} \tag{4}$$

where Di denotes the carbon emission quota for the *i-th* gas turbine unit (including gas turbines and GBs); λr denotes the quota coefficient for gas turbine units; P_{Ri} denotes the heat output of the *i-th* gas turbine unit; P_{Ei} denotes the electricity output of the *i-th* gas turbine unit; and β is the conversion factor for electricity.

C. CARBON TRADING MECHANISMS

In China, the carbon trading mechanism primarily manifests in two forms: traditional carbon trading and tiered carbon trading.

1) TRADITIONAL CARBON TRADING MECHANISM

The traditional carbon trading mechanism is a system in which, during a specified time period, a system entity can earn trading credits and sell them for profit if their carbon dioxide emissions do not exceed the emission quota. Otherwise, they are required to acquire additional emissions allowances.

Once the carbon emission rights quota and actual carbon emissions of the system have been established, it is possible to calculate the volume of actual carbon emission trading that occurs in the carbon trading market.

$$G_{IES,t} = G_{IES,a} + G \tag{5}$$

where $G_{IES,t}$ denotes the actual carbon emission trading volume engaged in the carbon trading market; G denotes the system's carbon emission rights quota; and $G_{IES,a}$ denotes the actual total carbon emissions of the system.

The representation of carbon trading cost is determined as follows:

$$F_C = \lambda \cdot G_{IES,t} \tag{6}$$

where F_C denotes the required payment for carbon trading expenses; and λ denotes the unit carbon emission trading price.

2) TIERED CARBON TRADING MECHANISM

The tiered carbon trading mechanism entails the segmentation of carbon dioxide emissions into multiple tiers or intervals. The higher the tier of carbon emissions, the higher the unit price for carbon emission trading, resulting in increased costs for the system. The expression for carbon trading cost is shown as follows:

$$F_C = \begin{cases} \lambda \cdot G_{IES,t} & 0 \le G_{IES,t} < l \\ \lambda \cdot (1+\mu) \cdot \left(G_{IES,t} - l\right) + \lambda \cdot l & l \le G_{IES,t} < 2l \\ \lambda \cdot (1+2\mu) \cdot \left(G_{IES,t} - 2l\right) + \lambda \cdot (2+\mu) \cdot l & 2l \le G_{IES,t} < 3l \\ \lambda \cdot (1+3\mu) \cdot \left(G_{IES,t} - 3l\right) + \lambda \cdot (3+3\mu) \cdot l & 3l \le G_{IES,t} < 4l \\ \lambda \cdot (1+4\mu) \cdot \left(G_{IES,t} - 4l\right) + \lambda \cdot (4+6\mu) \cdot l & G_{IES,t} \ge 4l \end{cases} \tag{7}$$

where F_C denotes the tiered carbon trading cost; λ stands for the base price of carbon trading; l denotes the length of the carbon emissions tier; and μ represents the increment in the price of tiered carbon trading.

3) REWARD-PENALTY TIERED CARBON TRADING MECHANISM

Reward-penalty tiered carbon trading mechanism incorporates reward-penalty coefficients into the tiered carbon trading system, which compares actual emissions with designated emissions in order to provide incentives or penalties. The unit price for purchasing carbon quotas increases as an entity surpasses its allocated quota, leading to additional punitive costs as a result of the tiered carbon pricing. Conversely, if the actual emissions do not surpass the allocated quota, any surplus carbon quotas can be traded in the carbon market, resulting in additional benefits.

Compared to the traditional carbon trading pricing mechanism, which is designed to further reduce carbon emissions, the reward-penalty tiered pricing mechanism di-vides multiple purchasing intervals. It introduces reward-penalty coefficients in addition to carbon trading, which aims to incentive energy-efficient initiatives by energy supply enterprises. These coefficients provide incentives or sanctions depending on the discrepancy between the actual and specified emission levels.

When a power company's carbon emissions decrease below the allocated carbon quotas, government departments provide specific technical subsidies as incentives. In this scenario, the cost of carbon trading for this portion can be expressed as follows:

$$F_C = \begin{cases} -\lambda \cdot (1+2\beta) \cdot \left(G_{IES,t} + 2l\right) - \lambda \cdot (2+\beta) \cdot l & G_{IES,t} \le -2l \\ -\lambda \cdot (1+\beta) \cdot \left(G_{IES,t} + l\right) - \lambda \cdot l & -2l < G_{IES,t} \le -l \\ -\lambda \cdot G_{IES,t} & -l \le G_{IES,t} < 0 \end{cases} \tag{8}$$

If a power company's actual carbon emissions surpass the allocated carbon quotas, the company is required to procure additional carbon quotas from the carbon trading market. The cost of carbon trading for this segment can be represented as follows:

$$F_C = \begin{cases} \lambda \cdot G_{IES,t} & 0 \le G_{IES,t} < l \\ \lambda \cdot (1+\alpha) \cdot \left(G_{IES,t} - l\right) + \lambda \cdot l & \\ & l \le G_{IES,t} < 2l \\ \lambda \cdot (1+2\alpha) \cdot \left(G_{IES,t} - 2l\right) + \lambda \cdot (2+\alpha) \cdot l & \\ & 2l \le G_{IES,t} < 3l \\ \lambda \cdot (1+3\alpha) \cdot \left(G_{IES,t} - 3l\right) + \lambda \cdot (3+3\alpha) \cdot l & \\ & 3l \le G_{IES,t} < 4l \\ \lambda \cdot (1+4\alpha) \cdot \left(G_{IES,t} - 4l\right) + \lambda \cdot (4+6\alpha) \cdot l & \\ & G_{IES,t} \ge 4l \end{cases} \tag{9}$$

where F_C denotes the cost of the reward-penalty tiered carbon trading; λ denotes the base price of carbon trading; l denotes the length of the carbon emissions tier; and α and β denote the reward and penalty coefficients in the reward-penalty tiered carbon trading, respectively.

4) EXPLANATION AND JUSTIFICATION OF KEY ASSUMPTIONS

Based on the previous introduction of various carbon trading mechanisms, this paper presents the relationships between carbon trading cost and carbon trading volume for the traditional carbon trading model, the tiered carbon trading model, and the reward-penalty tiered carbon trading model, as shown in Fig. 2.

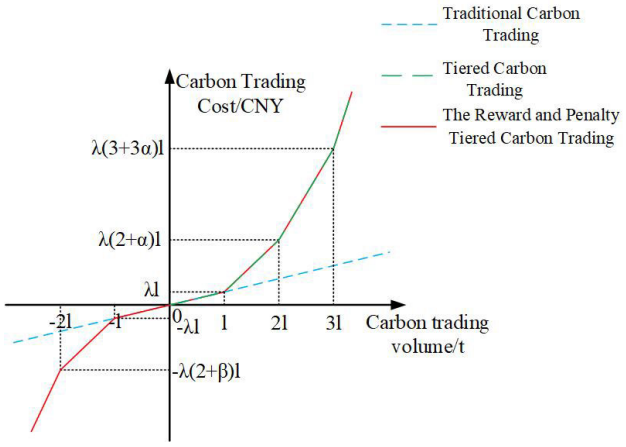

FIGURE 2. Relationship between carbon trading costs and trading volume.

From Fig. 2, it can be concluded that the tiered carbon trading mechanism performs better than the traditional carbon trading mechanism when the carbon trading volume is positive (system carbon emissions exceed the allocated carbon quota). The more the system emits carbon, the more carbon quotas need to be purchased, leading to higher carbon quota prices and increased economic costs for the system, while excessive carbon emissions are harmful to the environment. In this stage, the reward-penalty tiered carbon trading mechanism performs similarly to the tiered carbon trading mechanism.

The reward-penalty tiered carbon trading mechanism performs better than the traditional carbon trading mechanism when the carbon trading volume is negative (system carbon emissions are less than the allocated carbon quota). The less the system emits carbon, the more carbon quotas can be sold to the carbon market, resulting in higher selling prices for carbon quotas and increased revenue for the system, thereby reducing economic pressure. This tiered purchase price drives the energy system towards reducing carbon emissions.

Comparing the three carbon trading mechanisms, the reward-penalty tiered carbon trading mechanism outperforms both when the carbon trading volume is positive and negative. Therefore, this paper selects the reward-penalty tiered carbon trading mechanism as part of the objective function to be integrated into the CCHP system to reduce carbon emissions and enhance low-carbon economic performance.

III. ENERGY SYSTEM MODELING UNDER CARBON TRADING MECHANISM

The paper considers the varied energy requirements within the park and designs a CCHP system that integrates four energy sources: cooling, heating, electricity, and gas. The system incorporates a centralized power bus for the exchange of electrical power with the grid, as depicted in Fig. 3.

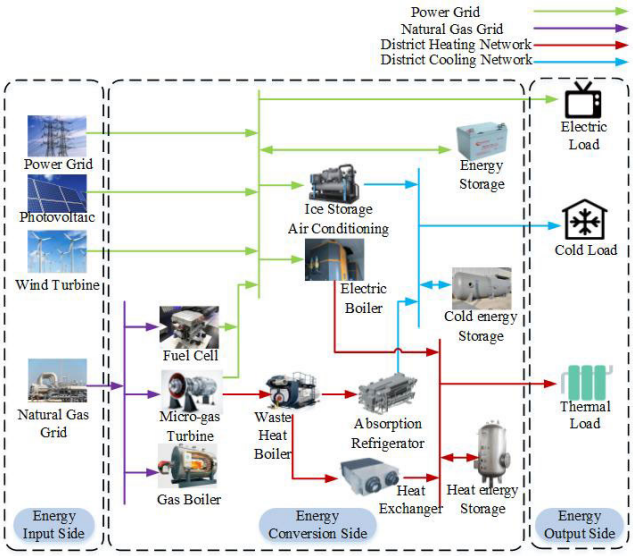

FIGURE 3. CCHP model.

The park's energy system is comprised of three primary components: energy input, energy conversion, and energy output. The energy input side primarily comprises photovoltaic (PV), wind turbine (WT), the power grid, and natural gas networks. The energy conversion side includes a variety of equipment such as fuel cell (FC), micro-gas

turbine (MT), gas boiler (GB), waste heat boiler (WHB), electric boiler (EB), ice-storage air-conditioning (ISAC), absorption refrigerator (AR), and heat exchanger (HE). Energy storage (ES) systems on the conversion side mainly consist of ES devices, cold energy storage (CS), and heat energy storage (HS). The energy output side addresses the necessary cooling, heating, and electrical demands.

The fuel consumption of MT can be estimated using a linear function [28]:

$$F_{MT}^{T} = \alpha_{Fi} \cdot P_{MT}^{T} + \beta_{Fi} \cdot U_{MT}^{T} \tag{10}$$

where P_{MT}^{T} denotes the output electrical power of MT during the *T-th* interval; U_{MT}^{T} denotes the on-off status indicator for MT; 0 and 1 denote the status of off and on, respectively; α_{Fi} and β_{Fi} denote the fuel coefficients for MT.

During the operation of MT system, the high-temperature waste flue gas is captured and utilized for heating and cooling purposes through WHB, HE, and AR. This paper does not take into account the effects of environmental factors and combustion efficiency on MT. The characteristic model of MT is obtained as follows:

$$\begin{cases} G_{MT}^{T} = \dfrac{P_{MT}^{T} \cdot (1 - \eta_{MT} - \eta_{L})}{\eta_{MT}} \\ H_{MT}^{T} = G_{MT}^{T} \cdot C_{OP,h}\eta_{h} \\ Q_{MT}^{T} = G_{MT}^{T} \cdot C_{OP,c}\eta_{c} \end{cases} \tag{11}$$

where G_{MT}^{T} denotes the waste heat from MT during the *T-th* interval; η_{MT} denotes the power generation efficiency of MT; η_{L} denotes the heat dissipation coefficient; H_{MT}^{T} and Q_{MT}^{T} denote the heat and cooling output of HE and AR during the *T-th* interval, respectively; $C_{OP,h}$ and η_{h} denote the heating coefficient and flue gas recovery rate of HE, respectively; $C_{OP,c}$ and η_{c} denote the cooling coefficient and flue gas recovery rate of AR, respectively.

The responsibility of electricity scheduling during daily operations will be assumed by FC. Consequently, this paper does not address the utilization of its waste heat. Its fuel consumption is given as follows [29]:

$$F_{FC}^{T} = \alpha_{c} \cdot P_{FC}^{T} + \beta_{c} \cdot U_{FC}^{T} \tag{12}$$

where P_{FC}^{T} denotes the output electrical power of FC during the *T-th* interval; U_{FC}^{T} denote the on-off status indicator for FC; 0 and 1 denote the status of off and on, respectively; α_{c} and β_{c} denote the fuel coefficients for FC.

ISAC system consists of chillers, cold storage tanks, and auxiliary equipment. This paper utilizes a parallel ISAC system [30], where ice storage is limited to off-peak elec-tricity pricing periods, and the chillers can provide cooling and store ice simultaneously. The power consumption formulas for each device can be available in Bao et al. [31]. The specific constraints are determined as follows:

$$\begin{cases} U_{a}^{T} \cdot Q_{a}^{min} \le Q_{a}^{T} \le U_{a}^{T} \cdot Q_{a}^{max} \\ 0 \le Q_{c}^{T} \le U_{c}^{T} \cdot Q_{a}^{max} \qquad U_{c}^{T} = 0, T \ne \Omega_{valley} \\ Q_{a}^{min} \le Q_{c}^{T} + Q_{a}^{T} \le Q_{a}^{max} \\ 0 \le Q_{d}^{T} \le U_{d}^{T} \cdot Q_{d}^{max} \qquad U_{d}^{T} = 0, T \ne \Omega_{valley} \end{cases} \tag{13}$$

where Q_{a}^{T} and Q_{c}^{T} denote the output cooling power and ice storage power of the chillers respectively; Q_{d}^{T} denotes the melting power of the cold storage tank; U_{a}^{T} and U_{c}^{T} denote the cooling and ice storage status flags of the chillers, respectively; U_{d}^{T} denotes the status flag of the cold storage tank; 0 and 1 denote the status of off and on, respectively; and Ω_{valley} denotes the set of all time periods during off-peak electricity pricing.

To capitalize on the low-carbon attributes of CCHP system, a reward-penalty tiered carbon trading mechanism has been implemented to constrain the system's carbon emissions. Given that the system exclusively procures electricity from thermal power sources from the external grid, the carbon emissions within CCHP system are primarily derived from three sources: purchased electricity from the upper-level grid, GB, and CHP. Both GB and CHP produce carbon dioxide as a byproduct of natural gas combustion. The quota method utilized in this paper involves the gratuitous allocation. Consequently, the distribution of complimentary carbon emission allowances for carbon trading is outlined as follows:

$$\begin{cases} G = G_{Grid} + G_{CHP} + G_{GB} \\ G_{Grid} = \varepsilon_{e} \cdot \sum_{t=1}^{T} P_{g,t}^{buy} \cdot \Delta t \\ G_{CHP} = \varepsilon_{h} \cdot \left(\sum_{t=1}^{T} \varphi_{e-h} \cdot P_{MT,t} + P_{WHB,t} \right) \cdot \Delta t \\ G_{GB} = \varepsilon_{h} \cdot \sum_{t=1}^{T} P_{GB,t} \cdot \Delta t \end{cases} \tag{14}$$

where denote G_{Grid}, G_{CHP}, and G_{GB} free carbon quotas for purchased electricity from the external grid (IES), CHP, and GB, respectively; G denotes the total carbon quota of IES; $P_{g,t}^{buy}$ denotes the purchased electricity amount from IES; ε_{e} and ε_{h} denote the free carbon quota coefficients per unit of electricity and per unit of the heat, respectively; φ_{e-h} denotes the conversion factor for transforming power generation into heat sup-ply, which is 6 MJ/(kWh) [32]; $P_{MT,t}$ denotes the output power of MT in the electric power; $P_{WHB,t}$ and $P_{GB,t}$ denote the heat output power of WHB and GB, respectively.

IV. MULTI-TIME-SCALE LAYERED OPTIMIZATION FOR CARBON EMISSION SCHEDULING

To mitigate the potential effects of uncertainties in renewable energy and load forecasting on the scheduling of CCHP systems, this study develops a multi-time scale optimization scheduling model that covers daily and intraday periods. Day-ahead scheduling achieves low-carbon economic benefits by

optimizing the system structure from a spatial dimension. The multi-time scale optimization scheduling strategy, on the other hand, leverages the advantage of increased prediction accuracy as the scheduling time scale decreases, reducing the impact of renewable energy and load uncertainties and equipment output fluctuations on the scheduling results. The multi-time scale optimization scheduling block diagram proposed in this paper is shown in Fig. 4.

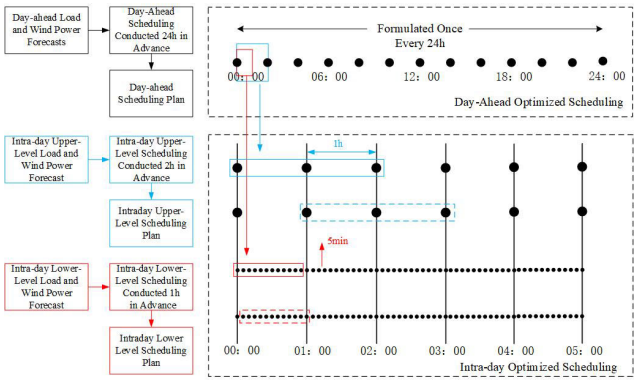

FIGURE 4. Multi-Time scale optimization scheduling block diagram.

(1) The daily scheduling phase operates on a 1-hour time scale with the objective of minimizing the combined costs of procurement, operational, and reward-penalty tiered carbon trading. It produces a 24-hour operational plan in advance for each device. The intraday rolling optimization scheduling follows the previous schedule and adjusts the forecast information within the subsequent control time domain, taking into account the variations in different energy sources at the scheduling time scale.

(2) Intraday rolling optimization scheduling shortens the prediction period based on day-ahead forecasting. Due to the different characteristics of various energies over different time scales, a dual-time scale scheduling strategy is used to balance power fluctuations of different energies, dividing the intraday rolling optimization scheduling into an upper and lower layer structure. The upper stratum is designed to mitigate extended fluctuations in thermal energy output and functions within a control time frame of 1 hour, with a scheduling window of 2 hours. The lower layer deals with shorter-term variations in electrical power, functioning within a control time domain of 5 minutes, with a scheduling window of 1 hour. Rolling optimization involves saving the optimization results from the previous control time domain. The second optimization starts from the next control domain using new forecast data, repeating the above optimization process in a rolling update fashion. Rolling optimization further enhances the system's low-carbon economic benefits and enhances its capacity to integrate new energy sources. Intraday rolling optimization aims to adjust the output of system energy devices to ensure smooth operation, progressively refining time scales to reduce the impact of generation and load power fluctuations on system optimization.

A. ADVANCED DAY-AHEAD SCHEDULING MODEL CONSIDERING A TIERED CARBON TRADING MECHANISM

1) TRADITIONAL CARBON TRADING MECHANISM

The scheduling model has recently been developed as a mixed-integer linear programming problem, aiming to minimize the total costs associated with procurement, operational maintenance, and stepwise carbon trading.

$$F = min\left(C_{NG} + C_{bt} + C_{grid} + F_C\right) \tag{15}$$

where F denotes the total cost of IES; C_{NG}, C_{bt}, C_{grid}, and F_C denote the procurement cost for gas, battery charge-discharge aging cost, electricity procurement cost, and stepwise carbon trading cost, respectively. The expression for ' F_C ' is expressed in Equation (8) and Equation (9), while the remaining three components are represented as follows:

$$\begin{cases} C_{bt} = \sum_{T=1}^{24} R_{bt}^T \cdot \left(U_{bt,dis}^T + U_{bt,chr}^T\right) \cdot \Delta T \\ C_{NG} = \sum_{T=1}^{24} R_{NG}^T \cdot \left(\dfrac{\sum_{i=1}^{n} F_{MT,i}^T + F_{GB}^T + F_{FC}^T}{H_{NG}}\right) \cdot \Delta T \\ C_{grid} = \sum_{T=1}^{24} R_{grid}^T \cdot P_{grid}^T \cdot \Delta T \end{cases} \tag{16}$$

where ΔT denotes the time interval; R_{bt}^T denotes the unit battery aging cost; $U_{bt,chr}^T$ and $U_{bt,dis}^T$ denote the charging and discharging status flags of the battery, respectively; 0 and 1 denote the status of off and on, respectively; R_{NG}^T denotes the purchase price of natural gas for the system in the *T-th* period; F_{MT}^T, F_{GB}^T, and F_{FC}^T denote the fuel consumption of MT, GB, and FC in the *T-th* period, respectively; H_{NG} denotes the lower heating value of natural gas; R_{grid}^T and P_{grid}^T denote the unit purchase price and the purchased power of electricity in the *T-th* period, respectively.

2) CONSTRAINTS

Taking into account the physical characteristics of the system's various devices and energy balance, the constraints that this paper needs to satisfy are as follows:

(1) Equipment operation constraints

The operational constraints for each device must comply with the minimum and maximum output levels as well as the maximum and minimum ramp rates. Specifically designed for MT as follows:

$$U_{MT}^T \cdot P_{MT}^{min} \le P_{MT}^T \le U_{MT}^T \cdot P_{MT}^{max} \tag{17}$$

$$P_{MT}^{down} \le P_{MT}^T - P_{MT}^{T-1} \le P_{MT}^{up} \tag{18}$$

where P_{MT}^{min} and P_{MT}^{max} denote the minimum and maximum output power of MT, respectively; P_{MT}^T denotes the output electrical power of MT in the *T-th* time interval; U_{MT}^T denotes

the start-stop status flag of MT; 0 and 1 denote the status of off and on, respectively; P_{MT}^{up} and P_{MT}^{down} denote the upper and lower ramp rate limits of MT, respectively.

To prevent negative impacts on battery lifespan caused by low power and low state of charge (SOC) during charge and discharge, it is essential for battery operation to comply with the limitations of charging, discharging, and SOC, which can be expressed as follows:

$$\begin{cases} U_{bt,chr}^{T} \cdot P_{bt,chr}^{min} \le P_{bt,chr}^{T} \le U_{bt,chr}^{T} \cdot P_{bt,chr}^{max} \\ U_{bt,dis}^{T} \cdot P_{bt,dis}^{min} \le P_{bt,dis}^{T} \le U_{bt,dis}^{T} \cdot P_{bt,dis}^{max} \end{cases} \tag{19}$$

$$\begin{cases} S_{SOC}^{T} = S_{SOC}^{T-1} + \left(\eta_{bt,chr} \cdot P_{bt,chr}^{T} - \dfrac{P_{bt,dis}^{T}}{\eta_{bt,dis}} \right) \cdot \Delta T \\ S_{SOC}^{min} \le S_{SOC}^{T} \le S_{SOC}^{max} \end{cases} \tag{20}$$

where S_{SOC}^{T} denotes SOC value of the battery; $P_{bt,chr}^{T}$ and $P_{bt,dis}^{T}$ denote the charging and discharging power of the battery, respectively; $\eta_{bt,chr}$ and $\eta_{bt,dis}$ denote the charging and discharging efficiency of the battery, respectively; ΔT denotes the time interval in the scheduling plan; $U_{bt,chr}^{T}$ and $U_{bt,dis}^{T}$ satisfy the mutually exclusive constraint and the charge-discharge frequency constraint (Equations (21) and (22)), respectively.

$$U_{bt,chr}^{T} + U_{bt,dis}^{T} \le 1 \tag{21}$$

$$\sum_{T=1}^{24} U_{bt,chr}^{T} + U_{bt,dis}^{T} \le T \tag{22}$$

During practical operation, the battery must comply with the charge-discharge ramp rate constraint as illustrated in Equation (23) as follows:

$$\begin{cases} P_{bt,chr}^{down} \le P_{bt,chr}^{T} - P_{bt,chr}^{T-1} \le P_{bt,chr}^{up} \\ P_{bt,dis}^{down} \le P_{bt,dis}^{T} - P_{bt,dis}^{T-1} \le P_{bt,dis}^{up} \end{cases} \tag{23}$$

where $P_{bt,chr}^{up}$, $P_{bt,chr}^{down}$, $P_{bt,dis}^{up}$ and $P_{bt,dis}^{down}$ denote the upper and lower ramp rate limits for the charging and discharging states of the battery.

When HE, HS, and EB are unable to attain thermal power balance status within the system, GB compensates for the shortfall. Therefore, it is necessary for GB to comply with the constraints illustrated in Equations (24) and (25).

$$H_{GB}^{T} = F_{GB}^{T} \cdot \eta_{GB} \tag{24}$$

$$H_{GB}^{min} \le H_{GB}^{T} \le H_{GB}^{max} \tag{25}$$

where F_{GB}^{T} denotes the natural gas consumption of GB in the *T-th* period; H_{GB}^{T} denotes the output thermal power of GB in the *T-th* period; and η_{GB} denotes the efficiency coefficient of GB.

EB utilizes surplus electricity during low-demand periods for heating, adhering to specified operational limits.

$$H_{EB}^{T} = P_{EB}^{T} \cdot \eta_{EB} \tag{26}$$

$$0 \le P_{EB}^{T} \le P_{EB}^{max} \tag{27}$$

where P_{EB}^{T} and H_{EB}^{T} denote the power consumption and output thermal power of EB in the *T-th* period, respectively; P_{EB}^{max} denotes the rated capacity of EB; and η_{EB} denotes the efficiency coefficient of EB.

The thermal storage tank has the capacity to store surplus heat energy when it is abundant and to release heat energy when there is an inadequate supply or when the cost of heat generation is high. This improves the operational flexibility and cost-effectiveness of the system, provided that the capacity constraints and charge-discharge thermal power constraints outlined in Equations (28) and (29) are met.

$$\begin{cases} W_{tst}^{T} = W_{tst}^{T-1} \cdot (1 - \gamma_h) + \left(\eta_{tst,chr} \cdot H_{tst,chr}^{T} - \dfrac{H_{tst,dis}^{T}}{\eta_{tst,dis}} \right) \\ W_{tst}^{min} \le W_{tst}^{T} \le W_{tst}^{max} \end{cases} \tag{28}$$

$$\begin{cases} U_{tst,chr}^{T} \cdot H_{bt,chr}^{min} \le H_{tst,chr}^{T} \le U_{tst,chr}^{T} \cdot H_{tst,chr}^{max} \\ U_{tst,dis}^{T} \cdot H_{tst,dis}^{min} \le H_{tst,dis}^{T} \le U_{tst,dis}^{T} \cdot H_{tstt,dis}^{max} \end{cases} \tag{29}$$

where W_{tst}^{T} denotes the stored thermal energy in the thermal storage tank; $H_{tst,chr}^{T}$ and $H_{tst,dis}^{T}$ denote the charging and discharging thermal power of the thermal storage tank, respectively; γ_h denotes the self-discharge rate of energy in the thermal storage tank; $\eta_{tst,chr}^{T}$ and $\eta_{tst,dis}^{T}$ denote the charging and discharging efficiencies of the thermal storage tank, respectively; $U_{tst,chr}^{T}$ and $U_{tst,dis}^{T}$ denote the charging and discharging status flags of the thermal storage tank, which is subject to the mutually exclusive constraint illustrated in Equation (30), respectively; and 0 and 1 denote the status of off and on, respectively.

$$U_{tst,chr}^{T} + U_{tst,dis}^{T} \le 1 \tag{30}$$

Similar to the operation mode of the battery, the thermal storage tank must adhere to the ramp rate constraints as indicated in Equation (31).

$$\begin{cases} H_{tst,chr}^{down} \le H_{tst,chr}^{T} - H_{tst,chr}^{T-1} \le H_{tst,chr}^{up} \\ H_{tst,dis}^{down} \le H_{tst,dis}^{T} - H_{tst,dis}^{T-1} \le H_{tst,dis}^{up} \end{cases} \tag{31}$$

where $H_{bt,chr}^{up}$, $H_{bt,chr}^{down}$, $H_{bt,dis}^{up}$ and $H_{bt,dis}^{down}$ denote the upper and lower ramp rate limits for the charging and discharging states of the thermal storage tank.

The chilled water tank is a crucial component of ISAC system. The model considers loss coefficients, refrigeration efficiency, and large storage capacity, while ensuring adherence to operational constraints depicted in Equations (32) and (33).

$$S_{ice}^{T} = S_{ice}^{T-1} \cdot (1 - \gamma_Q) + \left(\eta_{ice,chr} \cdot Q_c^{T} - \frac{Q_d}{\eta_{ice,dis}} \right) \tag{32}$$

$$S_{ice}^{down} \le S_{ice}^{T} - S_{ice}^{T-1} \le S_{ice}^{up} \tag{33}$$

where S_{ice}^{T} denotes the cooling capacity stored in the chilled water tank for the *T-th* time interval; γ_Q denotes the self-discharge coefficient; $\eta_{ice,chr}$ and $\eta_{ice,dis}$ denote the

coeffi-cients for ice storage and ice melting, respectively; S_{ice}^{up} and S_{ice}^{down} denote the upper and lower ramp rate limits for the chilled water tank, respectively.

(2) System constraints

In addition to the operational limitations of the equipment, the system must also adhere to constraints related to electrical, cooling, and heating power balance, as well as exchange power.

$$\begin{cases} P_{WT}^T + P_{PV}^T + \sum_{i=1}^{n} P_{MT,i}^T + P_{FC}^T + P_{grid}^T - P_{br,chr}^T \\ \quad + P_{br,dis}^T = P_{load}^T + P_{ISAC}^T + P_{EB}^T \\ \sum_{i=1}^{n} Q_{MT,i}^T + Q_a^T + Q_d^T = Q_{load}^T \\ \sum_{i=1}^{n} H_{MT,i}^T + H_{EB}^T + H_{GB}^T - H_{tst,chr}^T + H_{tst,dis}^T = H_{load}^T \end{cases} \tag{34}$$

where P_{WT}^T, P_{PV}^T, and P_{FC}^T denote the output power of WT, PV, and FC, respectively; P_{grid}^T denotes the purchased power; P_{ISAC}^T denotes the electricity consumption of ISAC in the *T-th* time interval; Q_{MT}^T denotes the cooling capacity of AR in the *T-th* time interval; Q_a^T and Q_d^T denote the cooling output power of ISAC's refrigeration unit and the ice melting power of ISAC's chilled water tank, respectively. H_{MT}^T denotes the cooling capacity of HE in the *T-th* time interval.

B. INTRADAY ROLLING OPTIMIZATION SCHEDULING MODEL

1) UPPER-LEVEL ROLLING OPTIMIZATION SCHEDULING MODEL

In the upper-level optimization problem, the adjustment of each micro-source's output is determined by the variation of thermal and cold loads at time t, in order to mitigate fluctuations in thermal and cold energy power, while adhering to the operational state of MT in advance and the thermal and cold scheduling strategy. The upper-level rolling optimization scheduling is designed to minimize the total of procurement costs, equipment adjustment penalty costs, and stepwise carbon trading costs, which are expressed as the objective function in Equation (35):

$$F_1 = min \sum_{t=k}^{k+M} C_{ISAC}^t + C_{NG}^t + C_{EB}^t + F_{C1} \tag{35}$$

where M denotes the control time domain of the thermal and cold scheduling; and C_{ISAC}^t, C_{NG}^t, C_{EB}^t, and F_{C1} denote the procurement cost of, gas, EB adjustment cost, and intraday stepwise carbon trading cost, respectively. The expression for 'F_{C1}' is expressed in Equation (8) and Equation (9), while the remaining three components are represented as follows:

$$\begin{cases} C_{ISAC}^t = \mu_{ISAC} \cdot \left(\Delta P_{ISAC}^t\right)^2 \cdot \Delta t \\ C_{NG}^t = \left[R_{NG}^t \cdot \left(\frac{F_{MT}^T + \Delta F_{MT}^t + F_{GB}^T + \Delta F_{GB}^t}{H_{NG}} \right) \right. \\ \quad \left. + \mu_{MT} \cdot \left(\Delta P_{MT}^t\right)^2 + \mu_{GB} \cdot \left(\Delta H_{GB}^t\right)^2 \right] \cdot \Delta t \\ C_{EB}^t = \mu_{EB} \cdot \left(\Delta P_{EB}^t\right)^2 \cdot \Delta t \end{cases} \tag{36}$$

where Δt denotes the time interval in the intraday scheduling; R_{NG}^t denotes the purchase price of natural gas for the system in the *t-th* interval; ΔF_{MT}^t and ΔF_{GB}^t denote the fuel consumption adjustment quantities for MT and GB in the *t-th* interval, respectively; ΔP_{MT}^t and ΔH_{GB}^t denote the adjustment power for MT and GB in the *t-th* interval, respectively; μ_{MT} and μ_{GB} denote the unit penalty costs for adjustment of MT and GB, respectively; μ_{EB} denotes the unit penalty cost for EB adjustment quantity; ΔP_{EB}^t denotes the adjustment power of EB in the *t-th* interval; μ_{ISAC} denotes the unit penalty cost for ISAC adjustment quantity; and ΔP_{ISAC}^t denotes the adjustment power of ISAC in the *t-th* interval.

The intraday thermal and cold energy scheduling must also adhere to power constraints for cold, hot, and MT, which can be expressed as follows:

$$\begin{cases} \sum_{i=1}^{n} Q_{MT,i}^t + Q_a^t + Q_d^t = Q_{load}^t \\ \sum_{i=1}^{n} H_{MT,i}^t + H_{EB}^t + H_{GB}^t - H_{tst,chr}^t + H_{tst,dis}^t = H_{load}^t \\ -0.05 P_{MT}^{max} \le \Delta P_{MT}^t \le 0.05 P_{MT}^{max} \end{cases} \tag{37}$$

2) LOWER-LEVEL ROLLING OPTIMIZATION SCHEDULING MODEL

In the lower-level optimization problem, the charge-discharge state of ES is taken into account in advance, and modifications are made to the previous schedule in response to fluctuations in renewable energy, electrical loads, and variations in the power of upper-level devices. The lower-level rolling optimization scheduling is designed to minimize both the procurement cost and the penalty cost associated with equipment adjustment, as depicted in Equation (38):

$$F_2 = min \sum_{t=k}^{k+N} C_{grid}^t + C_{FC}^t + C_{bt}^t + \beta \cdot \left(S_{SOC}^T - S_{SOC}^t\right)^2 \tag{38}$$

where N denotes the control time domain of the electrical energy scheduling; C_{grid}^t, C_{FC}^t, and C_{bt}^t denote the procurement cost of electricity, FC adjustment cost, and the cost associated with changes in the charging and discharging power of the battery, respectively; and β denotes the penalty factor for ES SOC. The remaining three components are

represented as follows:

$$\begin{cases} C_{grid}^{t} = \left[R_{grid}^{t} \cdot \left(P_{grid}^{T} + \Delta P_{grid}^{t} \right) + \mu_{grid} \cdot \left(\Delta P_{grid}^{t} \right)^{2} \right] \cdot \Delta t \\ C_{FC}^{t} = \left[C_{NG} \cdot \dfrac{F_{FC}^{T} + \Delta F_{FC}^{t}}{H_{NG}} + \mu_{FC} \cdot \left(\Delta P_{FC}^{t} \right)^{2} \right] \cdot \Delta t \\ C_{bt}^{t} = \mu_{p} \cdot \left[\left(\Delta P_{bt,dis}^{t} \right)^{2} + \right] \cdot \left(\Delta P_{bt,chr}^{t} \right)^{2} \Delta t \end{cases} \tag{39}$$

where R_{grid}^{t} denotes the electricity purchase price f or the system in the *t-th* interval; μ_{grid} denotes the unit penalty cost for exchange power adjustment quantity; ΔP_{grid}^{t} denotes the exchange power adjustment rate in the *t-th* interval; μ_{FC} denotes the unit penalty cost for FC adjustment quantity; ΔP_{FC}^{t} denotes the adjustment power of FC in the *t-th* interval; μ_{p} denotes the unit penalty cost for battery adjustment quantity; $\Delta P_{bt,chr}^{t}$ and $\Delta P_{bt,dis}^{t}$ denote the adjustment power for charging and discharging of the battery in the *t-th* interval, respectively.

The intraday electrical energy scheduling must adhere to constraints related to power balance, intraday SOC, and exchange power with the grid, which are shown as follows:

$$\begin{cases} P_{WT}^{t} + P_{PV}^{t} + \sum_{i=1}^{n} P_{MT,i}^{T} + P_{FC}^{t} + P_{grid}^{t} - P_{br,chr}^{t} \\ \quad + P_{br,dis}^{t} = P_{load}^{t} + P_{ISAC}^{t} + P_{EB}^{t} \\ C_{FC}^{t} = -0.05 S_{SOC}^{T} \le \Delta S_{SOC}^{t} \le 0.05 S_{SOC}^{T} \\ \quad -0.05 P_{grid}^{T} \le \Delta P_{grid}^{t} \le 0.05 P_{grid}^{max} \end{cases} \tag{40}$$

V. CASE STUDY

A. FUNDAMENTAL DATA

This paper conducts simulation experiments utilizing the park system depicted in Figure 3 as a case study. The simulation parameters are delineated in Table 1. The an-ticipated patterns for electricity, heat, and cooling demands, as well as wind power and PV power, are illustrated in Fig. 5. Time-of-use electricity rates are detailed in Table 2. The operational mode of ISAC includes daytime cooling operations and simultaneous ice storage and cooling during the night. The process of ice melting from the ice storage tank is limited to peak electricity pricing periods. This approach enables the micro-grid system to attain advantageous economic scheduling outcomes. Gurobi solver is utilized for both the day-ahead and intraday stages in this study.

B. DAY-AHEAD SCHEDULING RESULTS

The day-ahead scheduling provides a 24-hour operating plan for each device, allowing CCHP system to achieve optimal low-carbon and cost-effective operation based on this plan.

TABLE 1. Model parameters.

Parameters	Value
α_{F1}, β_{F1}	2.64, 66.2
α_{F2}, β_{F2}	2.7, 50
η_{L}	0.02
$C_{OP.h}$, $C_{OP.c}$	1.5, 0.95
η_{GB}	0.9
η_{EB}	0.93
$\eta_{tst,chr}$, $\eta_{tst,dis}$	0.98, 0.98
$\eta_{br,chr}$, $\eta_{br,dis}$	0.95, 0.95
$\eta_{ice,chr}$, $\eta_{ice,dis}$	0.67, 0.75
γ_{h}, γ_{O}	0.02
R_{NG}	0.6CNY/m3
H_{NG}	9.78KW/m3
P_{MT1}^{max}, P_{MT2}^{max}	600, 450
P_{MT1}^{min}, P_{MT2}^{min}	15
H_{GB}^{max}, H_{GB}^{min}	1400, 0
P_{EB}^{max}	1000
P_{grid}^{max}, P_{grid}^{min}	2100, 0
Q_{a}^{max}	500
Q_{c}^{max}	300
Q_{d}^{max}	120
$P_{br,chr}^{min}$, $P_{br,chr}^{max}$	0, 200
$P_{br,dis}^{min}$, $P_{br,dis}^{max}$	0, 200
$H_{tst,chr}^{min}$, $H_{tst,chr}^{max}$	0, 200
$H_{tst,dis}^{min}$, $H_{tst,dis}^{max}$	0, 150

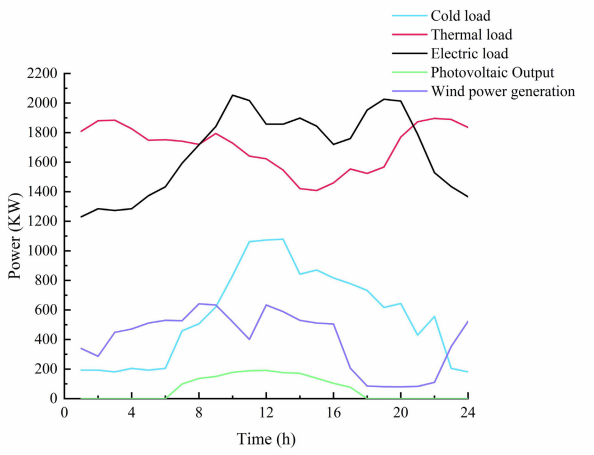

FIGURE 5. Predictive data for electrical, thermal, and cooling loads, alongside wind and PV energy.

TABLE 2. Schedule of electricity prices based on time-of-use.

Time		Price
peak	6:00-11:00 17:00-22:00	1.21
flat	11:00-17:00	0.73
valley	22:00-6:00	0.45

1) ANALYSIS OF LOW-CARBON PERFORMANCE AND ECONOMIC VIABILITY UNDER CARBON TRADING MECHANISM

The carbon trading price is established at 120 CNY per ton, with penalty and re-ward coefficients for tiered carbon

pricing set at 0.2 and 0.25, and a carbon trading volume interval of 1000 tons, leading to the resolution of the model.

To demonstrate the benefits of optimizing the scheduling of CCHP system and integrating the newly introduced reward-penalty tiered carbon trading mechanism to enhance economic and environmental efficiency, this study examines three scenarios:

Scenario 1 represents the baseline model where CCHP system's optimization does not account for carbon trading-associated costs.

Scenario 2 involves the incorporation of a traditional carbon trading mechanism into the optimization model of CCHP system.

Scenario 3 (the proposed scenario) incorporates the integration of a reward-penalty tiered carbon trading mechanism into the optimization model of CCHP system.

Scenario 4 Optimization Scheduling Model of CCHP Systems Considering Reward-Penalty Tiered Carbon Trading Mechanism, Utilizing Particle Swarm Algorithm for Optimal Operation.

The scheduling results under these four scenarios are compared and presented in Table 3.

TABLE 3. Comparison of day-ahead scheduling results under different operational scenarios.

scenarios	Carbon Trading Costs (in CNY)	Total Operating Costs (in CNY)
1	10085.70	57800
2	6364.58	54100
3	5621.39	53400
4	5684.64	53564

Table 3 illustrates that in comparison to Scenario 1, Scenario 2, which incorporates the traditional carbon trading mechanism, decreased carbon trading expenses by 36.90% and total costs by 6.40%. The decrease in emissions is ascribed to the incorporation of carbon trading expenses in the goal function, leading to stricter regulation of emissions and modifications in unit production, thereby reducing total expenses.

The results presented in Table 3 provide additional evidence that Scenario 3, in comparison to Scenario 2, resulted in a further reduction of 11.68% in carbon trading costs and a 1.29% decrease in total costs. The enhancement can be attributed to the implementation of a reward-penalty tiered carbon trading mechanism in Scenario 3, which has facilitated a more efficient control of emissions through the imposition of higher carbon trading prices. This mechanism enabled the optimization of unit power output, leading to a reduction in carbon trading costs and subsequently lowering the overall system costs.

Comparing Scenario 3 and Scenario 4 reveals that under unchanged system conditions, the optimal results obtained using Gurobi solver and Particle Swarm Algorithm are similar. However, Gurobi solver demonstrates distinct advantages in terms of solution speed, stability, guarantee of global optimality, debugging, maintenance, and scalability.

In summary, the proposed optimization scheduling method for CCHP systems considering reward-penalty tiered carbon trading mechanism not only enhances energy efficiency and achieves economic and low-carbon performance of CCHP systems but also offers advantages in solution speed, accuracy, and operational feasibility.

2) ANALYSIS RESULTS OF SOURCE-LOAD SCHEDULING BALANCE STATUS

The analysis in Section V-B1 demonstrates that the tiered carbon trading mechanism, which incorporates reward-penalty aspects, more effectively improves the park's energy utilization with higher efficiency. Therefore, this section is dedicated to analyzing the results of the day-ahead optimization for Scenario Three. The scheduling out-comes are depicted in Fig. 6 to 8.

Based on the electricity load balance status depicted in Fig. 6, the electricity load remains consistently low during the off-peak period from 22:00 to 06:00. The out-put of renewable energy gradually increases over this period, with the primary load being supported by point of common coupling (PCC). During the peak period from 06:00 to 11:00, there is a steady increase in electricity load. The output from both MT and FC demonstrates a continuous increase, eventually reaching a state of full load operation for a certain period. During this period, ES and the low power-consuming chilled water tank initiate the release of energy to decrease the system's reliance on the external power grid.

During the standard pricing period from 11:00 to 17:00, there is a gradual decrease in electricity demand. MT gradually reduces its output, resulting in a decrease in thermal and cooling energy supply.

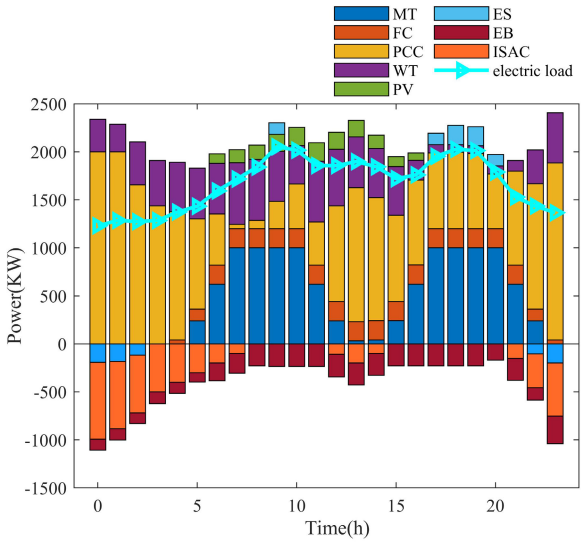

FIGURE 6. Analysis results of electricity load balance status.

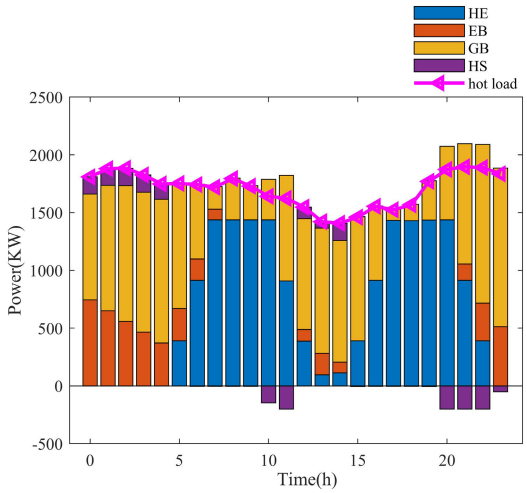

FIGURE 7. Analysis results of hot load balance status analysis results.

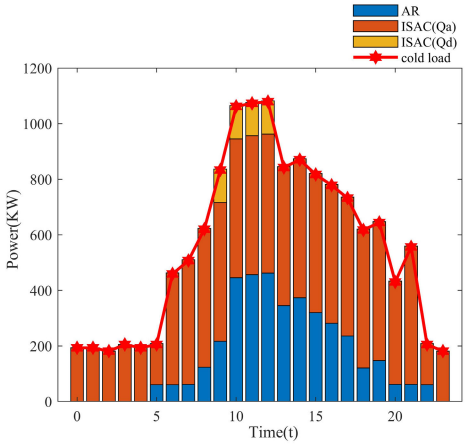

FIGURE 8. Analysis results of cooling load balance status.

The second peak period in electricity pricing occurs between 17:00 and 22:00. The operational status of the system reflects that of the 06:00 to 11:00 period. However, due to the reduced output of wind energy at this time, the frequency of discharging ES system is higher compared to the first peak pricing period.

The thermal load balance status, as illustrated in Fig. 7, indicates that during the off-peak period from 22:00 to 06:00, the thermal load is predominantly sustained by GB and EB. During the peak period from 06:00 to 11:00, there is a strategy in place to decrease the system's reliance on the external power grid by storing excess thermal energy using the HS equipment, which in turn reduces the conversion power of EB.

During the standard pricing period from 11:00 to 17:00, when the supply of thermal energy from MT decreases, HS equipment initiates the release of thermal energy.

During the time frame of 17:00 to 22:00, which signifies the second peak period for electricity pricing, the operational status of the system closely mirrors that of the 06:00 to 11:00 period.

With respect to the cooling load balance status (Fig. 8), the cooling load remains at a low level during the off-peak period from 22:00 to 06:00, primarily supported by ISAC.

During the standard pricing period from 11:00 to 17:00, the cooling capacity of AR increases as a result of the reduced thermal energy supplied by MT.

During the time frame of 17:00 to 22:00, which signifies the second peak period for electricity pricing, the operational status of the system is essentially comparable to that of the 06:00 to 11:00 period.

C. ANALYSIS RESULTS OF INTRADAY SCHEDULING MODEL

1) ANALYSIS OF THE EFFECTIVENESS OF MULTI-TIME SCALE MODELS

Using the optimization scheduling algorithm proposed in this study, combined with the conditions of Scenario Three, the multi-time scale optimization scheduling results are presented in Table 4.

TABLE 4. Multi-time scale optimization scheduling results.

	Day-ahead	Intraday
Wind power integration capacity/kW	397.36	398.49
Photovoltaic integration capacity/kW	219.91	220.53
Wind power integration rate/%	96.80	98.81
Photovoltaic integration rate/%	97.50	99.38

To verify the enhancement of renewable energy integration capacity through multi-time scale optimization, calculations were conducted to determine the integration capacities of wind and photovoltaic (PV) power as shown in Table 4. As indicated in Table 4, under multi-time scale scheduling, both wind and PV integration capacities have significantly improved. The integration rate of wind power reached 98.61%, which is 2.01% higher than that achieved with previous day scheduling. Similarly, the PV integration rate reached 99.38%, an improvement of 1.88% compared to previous day scheduling. These results demonstrate that multi-time scale scheduling effectively enhances the integration capacity of renewable energy sources.

2) COMPARISON AND ANALYSIS OF OUTPUT ADJUSTMENT FOR VARIOUS EQUIPMENT BETWEEN B. DAY-AHEAD AND INTRADAY PERIODS

The implementation of carbon trading mechanisms incentives the adoption of renewable energy sources within the system. However, the day-ahead scheduling plans rely on hourly

time scales, resulting in substantial fluctuations in system power. Consequently, this study aims to rectify the inaccuracies stemming from day-ahead predictions by implementing intraday forecasting adjustments. Concurrently, it regulates the output of equipment to minimize the negative impact of fluctuations in renewable energy power on the park's energy system. The optimization scheduling algorithm presented in this paper is employed in combination with the conditions specified in Scenario Three to illustrate the intraday optimized scheduling results in Fig. 9 to 14.

With respect to the scheduling of upper-level thermal energy, Fig. 9 demonstrates that EB follows the day-ahead operational plan, while also making slight modifications in response to real-time heat demand. During periods of low electricity prices, the system boosts its output to accumulate excess heat load for utilization during peak electricity pricing. Fig. 10 demonstrates that GB conforms to the day-ahead operational plan, with minor modifications made in response to real-time heat demand in order to promptly fulfill user heat load requirements. Fig. 11 illustrates that ISAC adheres to the day-ahead operational plan, with slight modifications made in response to real-time cooling demand. During periods of low electricity prices, the system in-creases its output and stores excess cooling load for use during peak electricity pricing.

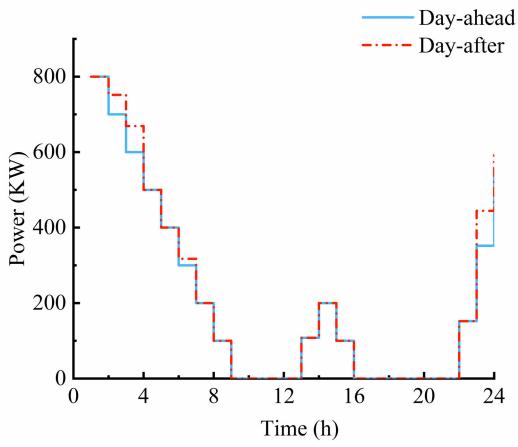

FIGURE 9. EB output power.

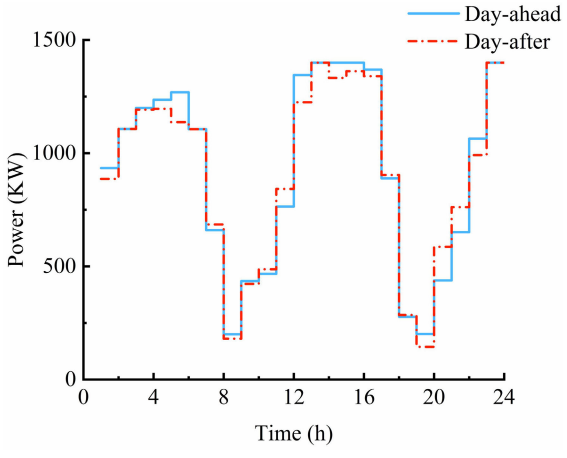

FIGURE 10. GB output power.

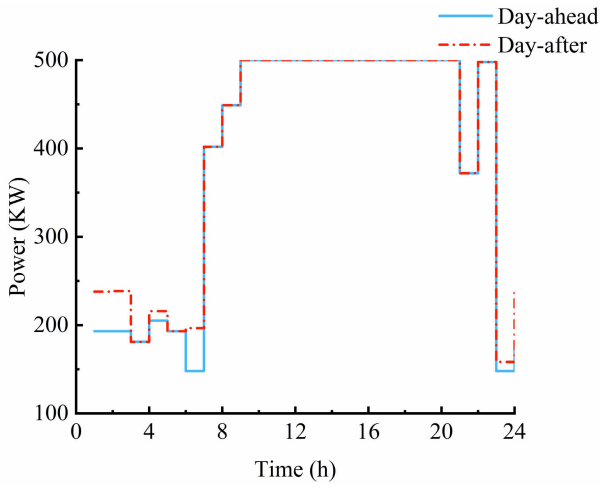

FIGURE 11. ISAC(Q_a) output power.

For lower-level electricity scheduling, Fig. 12 illustrates that MT adheres to the day-ahead operational plan and implements real-time adjustments in response to the system load in order to promptly fulfill the system's electricity demand. Fig. 13 presents the scheduling outcomes for grid interaction power, demonstrating a decrease in the system's electricity procurement curve during periods of peak pricing. The curves representing flat and low pricing periods are modified according to real-time demand. During periods of peak pricing, the reduction of purchased electricity through the use of stored loads can result in a decrease in the daily operating costs of the system. During the intraday scheduling stage, the management of system power fluctuations is primarily handled by FC, as illustrated in Fig. 14, in order to take into account the service life of ES and the stable operation of the external power grid. The implementation of a multi-timescale

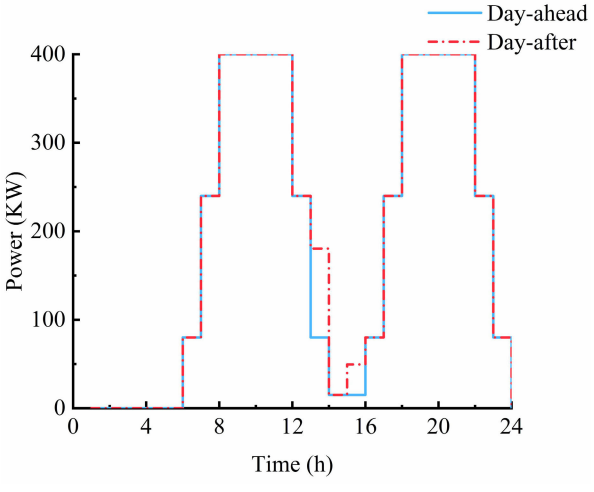

FIGURE 12. MT output power.

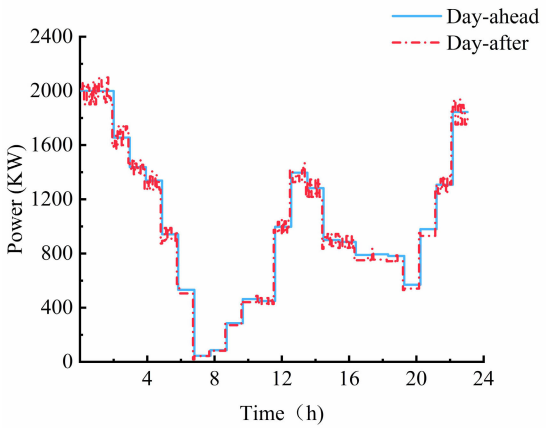

FIGURE 13. Grid power exchange.

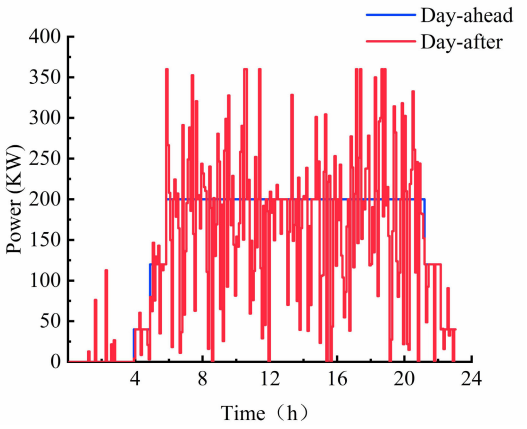

FIGURE 14. FC output power.

operational strategy serves to promptly mitigate user load fluctuations and minimize significant fluctuations in equipment output, thereby ensuring both economical and stable equipment operation.

D. ANALYSIS OF KEY PARAMETERS IN CARBON TRADING MECHANISM

The analysis conducted in the initial section of this paper demonstrates the interdependence between carbon trading prices and total costs. Consequently, this study manipulates the carbon trading price in Scenario Three to assess its influence on carbon trading expenses, overall costs, and other related factors. The findings are illustrated in Fig. 15. The figure illustrates that the optimization algorithm proposed in this paper results in a pattern where, as the carbon trading price gradually increases, both carbon trading costs and total costs initially experience an upward trend followed by a subsequent decline. The fluctuation in carbon trading expenses has an impact on the overall costs, reaching its peak when the carbon price reaches approximately 120 CNY per ton.

The analysis presented in Fig. 15 illustrates that a continuous rise in carbon trading prices ideally results in a reduction in both carbon trading costs and total costs. However, in cases

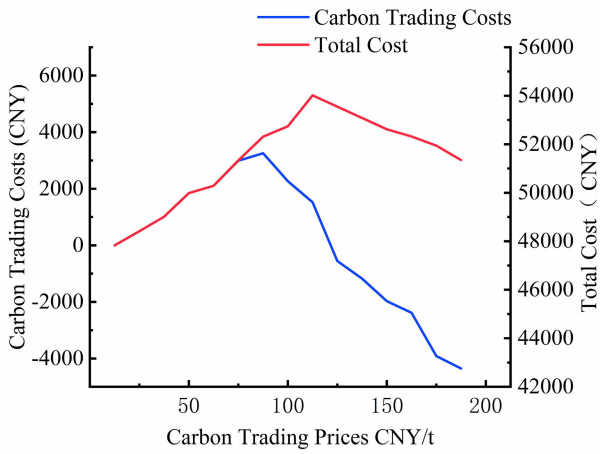

FIGURE 15. Cost mechanism analysis relative to carbon price fluctuations.

where the costs of carbon trading exhibit excessively high negative values, signifying an excessive dependence on the sale of carbon emissions for significant financial gains, this approach loses its effectiveness in controlling carbon emissions. Therefore, the pursuit of high profits through the exclusive sale of carbon emission rights is not in line with real market dynamics. Therefore, it would be suitable to establish a ceiling for the carbon trading price at 200 CNY per ton.

In energy systems that integrate the incentive-driven carbon trading mechanism, the incentive coefficient plays a critical role in influencing the system's ability to operate with low carbon emissions. Thus, this paper establishes the critical carbon price CC0 as the price at which emissions equal the quota, leading to zero carbon trading when emissions and quotas are in balance. Taking into account the influence of the incentive coefficient and a carbon emission interval length l of 1000 tons, diverse dis-patch models are resolved using different incentive coefficients, resulting in the findings depicted in Fig. 16.

The data presented in Figure 16 indicates that an elevated incentive coefficient is associated with a more rapid decline in carbon emissions as carbon prices rise, leading to a reduction in the critical carbon price as the incentive coefficient increases. For ex-ample, when the incentive coefficient is set to 0, the critical carbon price is estimated to be around 120 CNY per ton. However, when the incentive coefficient is 0.1, the critical carbon price decreases to 100 CNY per ton, and further reduces to 85 CNY per ton as the incentive coefficient reaches 0.2.

The carbon trading system operates on the principle of 'total control and trade', where quotas represent the targeted total emissions for a specific period in a given area. The critical carbon price is the minimum price required to achieve emission targets. As a result, this paper establishes the critical carbon price as the baseline reasonable carbon price. The analysis presented in Fig. 16 suggests that the critical carbon price gradually decreases as the incentive coefficient increases. Consequently, in energy systems that utilize penalty-based carbon trading

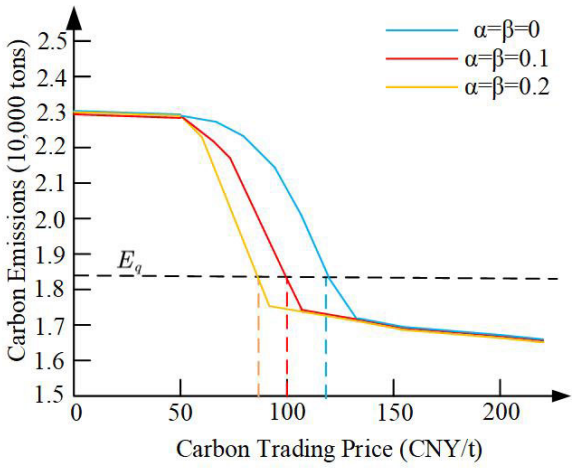

FIGURE 16. Comparative analysis of carbon emissions relative to carbon price and incentive coefficients.

mechanisms, appropriately increasing the incentive coefficient can lead to a more convergent carbon price range, thereby facilitating the achievement of emission reduction targets within a lower baseline carbon price range.

VI. CONCLUSION

This paper examines the influence of carbon trading mechanisms on a district energy system, using a system that encompasses cooling, heating, electricity, and gas as a case study. Given the low-carbon economic attributes and the diverse time scales associated with various energy sources in district energy systems, it is suggested a multi-time scale optimization and scheduling approach for district energy systems within the framework of a reward-penalty tiered carbon trading mechanism. The conclusions derived from simulation experiments are as follows:

1) The multi-time-scale rolling optimization scheduling method for the CCHP park, which considers carbon trading costs, can reduce carbon emissions while controlling the total cost increase during the day-ahead stage. During the intraday stage, it adjusts the output of each unit to mitigate the impact of source-load fluctuations on the system. Compared to conventional scheduling models, the proposed model better meets the requirements for environmental benefits, economic efficiency, and stability, providing valuable insights for the future application of low-carbon scheduling in power systems.

2) By incorporating the reward-penalty tiered carbon trading mechanism into the multi-time-scale optimization model, this paper compares the impact of no carbon trading mechanism, traditional carbon trading mechanism, and the reward-penalty tiered carbon trading mechanism on the system's economic and environmental performance. The results validate the superiority of the reward-penalty tiered carbon trading mechanism in reducing system costs and carbon emissions.

3) This paper analyzes the impact of two key parameters—carbon trading price and reward-penalty coefficient—on the carbon trading model of the CCHP system. It concludes that carbon trading price affects the system's carbon emissions, carbon trading costs, and total costs, and should be set within a reasonable range. Increasing the reward-penalty coefficient appropriately can make the system's response to carbon price changes more sensitive, further narrowing the reasonable range of carbon prices and achieving the desired emission reduction targets at a lower base carbon price.

In conclusion, the proposed optimization scheduling method effectively reduces the system's carbon emissions, maximizes economic benefits, and improves the stability and reliability of system operation. However, the reliability of the scheduling results may be affected by data inaccuracies, such as renewable energy generation forecasts and load demands. Additionally, the multi-time-scale optimization model increases computational complexity, potentially requiring significant computational power to avoid delays in computation time in practical applications. Future research could explore the introduction of more intelligent algorithms, such as deep learning and reinforcement learning, to enhance the accuracy and efficiency of optimization scheduling. Further studies could also investigate the collaborative optimization of the CCHP system with other energy systems, such as electric vehicle charging networks and energy storage systems, to comprehensively improve the overall efficiency and stability of the energy system.

REFERENCES

[1] L. Wang, "The historical background, significance and change path of China's proposed dual carbon goal," *HNU J. Soc. Sci.*, vol. 76, no. 3, pp. 41–45, Feb. 2023.
[2] C. Q. Kang, E. S. Du, Y. W. Li, N. Zhang, Q. X. Chen, H. Y. Guo, and P. Wang, "Key scientific problems and research framework for carbon perspective research of new power systems," *Power Syst. Technol.*, vol. 46, no. 3, pp. 21–33, Mar. 2022.
[3] Q. X. Chen, C. Q. Kang, Q. Xia, and K. Daniel, "Mechanism and modelling approach to low-carbon power dispatch," *Autom. Elect. Power Syst.*, vol. 34, no. 12, pp. 18–23, Jun. 2010.
[4] A. Xuan, X. Shen, Q. Guo, and H. Sun, "Two-stage planning for electricity-gas coupled integrated energy system with carbon capture, utilization, and storage considering carbon tax and price uncertainties," *IEEE Trans. Power Syst.*, vol. 38, no. 3, pp. 2553–2565, May 2023.
[5] F. Yao, J. W. Wang, F. S. Wen, and X. Y. Zhao, "Economic dispatch for a power system containing wind power and energy storage with carbon tax considered," *J. Electr. Power Sci. Technol.*, vol. 34, no. 1, pp. 38–46, Mar. 2019.
[6] H. Wu, S. F. Dong, X. L. Zhang, B. Nan, Y. Liu, and J. P. Nan, "Optimal dispatching of power system with wind power considering carbon trading mechanism," *Power Syst. Technol.*, vol. 48, no. 1, pp. 70–80, Aug. 2023.
[7] T. Yang, H. Liu, J. Wang, Z. S. Dang, Y. N. Geng, and H. B. Pen, "Deep reinforcement learning-based low-carbon economic dispatch of park integrated energy system," *Power Syst. Technol.*, vol. 1, pp. 1–11, Nov. 2023.
[8] X. P. Zhu, M. H. Liu, Q. Jiang, H. W. Luo, W. T. You, and H. Wen, "Low carbon economic scheduling of P2G integrated energy system considering demand response and carbon trading," *Electr. Meas. Instrum.*, vol. 1, pp. 1–9, May 2022.
[9] K. Y. Wang, Y. Liang, and R. Jia, "Low-carbon economical dispatch of the combined cooling heating and power microgrid considering shared energy storage," *Power Syst. Clean Energy*, vol. 38, no. 11, pp. 155–162, Nov. 2022.
[10] X. Zhou, X. Q. Han, Y. Z. L. Li, T. J. Li, and B. Y. Yan, "Low-carbon economic dispatch strategy for multi-agent integrated energy system based on adjustable thermoelectric ratio and two-stage stepped carbon trading," *Proc. CSU Electr. Power Syst. Assoc.*, vol. 35, no. 11, pp. 10–21, Nov. 2023.

[11] L. M. Wang, X. M. Liu, Y. Li, D. Chang, and X. Ren, "Low-carbon optimal dispatch of integrated energy system considering demand response under the tiered carbon trading mechanism," *Electr. Power Constr.*, vol. 45, no. 2, pp. 102–114, Oct. 2023.
[12] G. Lv, Y. Y. Zhang, J. Zhu, L. Liu, Y. H. Wu, and T. Wang, "Low-carbon optimal operation of electricity-heat-gas systems based on bi-directional tiered-pricing carbon trading," in *Proc. CFEEE*, 2023, pp. 377–387.
[13] T. Li, Q. Xiao, H. Jia, Y. Mu, X. Wang, W. Lu, and T. Pu, "Multi-agent schedule optimization method for regional energy Internet considering the improved tiered reward and punishment carbon trading model," *Frontiers Energy Res.*, vol. 10, pp. 1–12, May 2022.
[14] P. H. Jiao, X. Cai, L. L. Wang, J. J. Chen, Y. L. Zhao, and Y. F. Cao, "Flexibility operation for integrated energy system considering hydrogen energy under inertia characteristics and stepped carbon trading mechanism," *Sustain. Cities Soc.*, vol. 98, Nov. 2023, Art. no. 104809.
[15] X. Liu, X. Li, J. Tian, G. Yang, H. Wu, R. Ha, and P. Wang, "Low-carbon economic dispatch of integrated electricity-gas energy system considering carbon capture, utilization and storage," *IEEE Access*, vol. 11, pp. 25077–25089, 2023.
[16] K. Tang, S. Fang, G. Chen, and T. Niu, "Unit maintenance strategy considering the uncertainty of energy intensive load and wind power under the carbon peak and carbon neutral target," *IEEE Access*, vol. 11, pp. 38819–38827, 2023.
[17] P. Chen, C. Qian, L. Lan, M. Guo, Q. Wu, H. Ren, and Y. Zhang, "Shared trading strategy of multiple microgrids considering joint carbon and green certificate mechanism," *Sustainability*, vol. 15, no. 13, p. 10287, Jun. 2023.
[18] Y. Yang, Z. Luo, X. Yuan, X. Lv, H. Liu, Y. Zhen, J. Yang, and J. Wang, "Bi-level multi-objective optimal design of integrated energy system under low-carbon background," *IEEE Access*, vol. 9, pp. 53401–53407, 2021.
[19] W. Zhou, Y. Sun, X. Zong, H. Zhou, and S. Zou, "Low-carbon economic dispatch of integrated energy system considering carbon trading mechanism and LAES-ORC-CHP system," *Frontiers Energy Res.*, vol. 11, pp. 1–16, Mar. 2023.
[20] Z. Wang, W. K. Cai, J. X. Meng, Y. Y. Wu, and D. Wu, "Research on hybrid time scale rolling optimal operation of CCHP system with photovoltaic and energy storage," *J. Chin. Soc. Power Eng.*, vol. 43, no. 7, pp. 930–940, Jul. 2023.
[21] Z. Y. Chen, B. Y. Wen, and Z. S. Zhu, "Multi-time scale optimal scheduling of regional integrated energy system considering wind power correlation," *Elector. Power Autom. Equip.*, vol. 43, no. 8, pp. 25–32, Aug. 2023.
[22] W. Zhou, H. J. Tao, W. K. Cai, L. Zhang, and J. X. Meng, "Optimal scheduling research of multi-time-scale rolling optimization in CCHP system," *Acta Energ. Solaris Sin.*, vol. 44, no. 2, pp. 298–308, Feb. 2023.
[23] Z. Luo, Z. Zhu, Z. Zhang, J. Qin, H. Wang, Z. Gao, and Z. Yang, "Multi-Time-Scale rolling optimal dispatch for grid-connected AC/DC hybrid microgrids," *Processes*, vol. 7, no. 12, p. 961, Dec. 2019.
[24] L. Chen, X. Zhu, J. Cai, X. Xu, and H. Liu, "Multi-time scale coordinated optimal dispatch of microgrid cluster based on MAS," *Electr. Power Syst. Res.*, vol. 177, Dec. 2019, Art. no. 105976.
[25] J. Hou, W. Yu, Z. Xu, Q. Ge, Z. Li, and Y. Meng, "Multi-time scale optimization scheduling of microgrid considering source and load uncertainty," *Electric Power Syst. Res.*, vol. 216, Mar. 2023, Art. no. 109037.
[26] S. Zhang, Q. Wu, J. Chen, H. Zhang, and B. Pan, "Intra-day multi-time-scale hierarchical rolling scheduling of integrated energy system considering uncertainty," in *Proc. 5th Asia Energy Electr. Eng. Symp. (AEEES)*, Mar. 2023, pp. 1778–1782.
[27] Z. Cheng, D. Jia, Z. Li, J. Si, and S. Xu, "Multi-time scale dynamic robust optimal scheduling of CCHP microgrid based on rolling optimization," *Int. J. Electr. Power Energy Syst.*, vol. 139, Jul. 2022, Art. no. 107957.
[28] H. Cho, P. J. Mago, R. Luck, and L. M. Chamra, "Evaluation of CCHP systems performance based on operational cost, primary energy consumption, and carbon dioxide emission by utilizing an optimal operation scheme," *Appl. Energy*, vol. 86, no. 12, pp. 2540–2549, Dec. 2009.
[29] L. M. Wang, X. M. Liu, Y. Li, D. Chang, and X. Ren, "Optimization on microgrid with combined heat and power system," *Proc. China Soc. Electr. Eng.*, vol. 35, no. 14, pp. 102–114, Jul. 2015.
[30] S. Cheng, T. L. Huang, and R. Z. Wei, "Multi-time scale optimal scheduling of CCHP microgrid with Ice-storage air-conditioning," *Proc. China Soc. Electr. Eng.*, vol. 43, no. 5, pp. 30–38, Mar. 2019.
[31] Z. Bao, Q. Zhou, Z. Yang, Q. Yang, L. Xu, and T. Wu, "A multi time-scale and multi energy-type coordinated microgrid scheduling solution—Part I: Model and methodology," *IEEE Trans. Power Syst.*, vol. 30, no. 5, pp. 2257–2266, Sep. 2015.
[32] X. H. Zheng, X. Y. Liu, and J. Q. Zhong, "Integrated energy system planning considering a reward and punishment ladder-type carbon trading and electric-thermal transfer load uncertainty," *Proc. China Soc. Electr. Eng.*, vol. 40, no. 19, pp. 6132–6142, Oct. 2020.

TIANYI MA was born in Jilin, China, in 1986. She received the B.S. degree in electrical engineering and the Ph.D. degree in power electronics and power transmission from Beijing Jiaotong University, in 2008 and 2014, respectively.

She is currently a Professor with Beijing Institute of Graphic Communication. Her current research interests include the modeling and control of smart grids and intelligent equipment.

YILIN WANG was born in Shandong, China, in 1999. She received the B.S. degree in automation from Beijing Institute of Graphic Communication, Beijing, China, in 2022, where she is currently pursuing the M.S. degree in mechanical engineering.

Her research interests include multi-energy microgrid and integrated energy system planning and operation.

TING LI (Member, IEEE) was born in Shandong, China, in 1990. She received the B.S. degree in power systems and its automation from Shandong Agricultural University, the M.S. degree in control theory and control engineering from Shenyang University of Chemical Technology, in 2016, and the Ph.D. degree in control theory and control engineering from Northeastern University, in 2021.

She is currently a Teacher with Beijing Institute of Graphic Communication. Her current research interests include reinforcement learning, optimization control of complex nonlinear systems, adaptive control, and event-triggered control.

YUHAO ZHANG was born in Heilongjiang, China, in 2000. He received the B.S. degree in electrical engineering and its automation from Lanzhou Institute of Technology, in 2022. He is currently pursuing the M.S. degree in mechanical engineering with Beijing Institute of Graphic Communication, Beijing, China.

His research interests include machine learning and new energy forecasting.

ZHIYUAN WANG was born in Hebei, China, in 2001. He received the B.S. degree in electrical engineering and its automation from Hebei University of Architecture, in 2023. He is currently pursuing the M.S. degree in mechanical engineering with Beijing Institute of Graphic Communication, Beijing, China.

His research interest includes control and stability molecules for smart grids.